Adaptive Mammographic Image Enhancement Using First Derivative and Local Statistics

Jong Kook Kim, Jeong Mi Park, Koun Sik Song, and Hyun Wook Park*

***Abstract*—This paper proposes an adaptive image enhancement method for mammographic images, which is based on the first derivative and the local statistics. The adaptive enhancement method consists of three processing steps. The first step is to remove the film artifacts which may be misread as microcalcifications. The second step is to compute the gradient images by using the first derivative operators. The third step is to enhance the important features of the mammographic image by adding the adaptively weighted gradient images. Local statistics of the image are utilized for adaptive realization of the enhancement, so that image details can be enhanced and image noises can be suppressed. The objective performances of the proposed method were compared with those by the conventional image enhancement methods for a simulated image and the seven mammographic images containing real microcalcifications. The performance of the proposed method was also evaluated by means of the receiver operating-characteristics (ROC) analysis for 78 real mammographic images with and without microcalcifications.**

***Index Terms*—Adaptive image enhancement, contrast improvement ratio, first derivative, local statistics, mammographic image, receiver operating-characteristics analysis.**

I. Introduction

BREAST cancer is one of the major causes of mortality increase to middle-aged women, especially in developed countries [1]. Currently, it is well known that mammography is the most effective method for early detection of breast cancer. However, it is very difficult to interpret the X-ray mammograms because of the small differences in image density of various breast tissues, in particular, for dense breasts [2]. A possible sign of breast cancer is the appearance of clustered microcalcifications whose individual particles are usually under 0.5 mm in diameter with irregular and heterogeneous shape [3]. Individual microcalcifications are difficult to be detected because they are variable in shape as well as in size and may be embedded in areas of dense parencymal tissues. Therefore, careful diagnosis should be performed for the clustered microcalcifications that may herald an early-stage cancer. To improve the visibility of mammographic lesions on a computer monitor, image enhancement methods for digitized mammograms have been attempted by several researchers [4]–[9]. Image enhancement is usually performed by emphasizing image details and suppressing noises.

This paper proposes an adaptive image enhancement method in order to improve the visibility of low-contrast features while suppressing the noises. The adaptive image enhancement method exploits the first derivative operations using the Sobel operators [10], [11] or the compass operators [10], [12], and the local statistics of a mammographic image are used for an adaptive realization. The objective performance of the proposed method was compared with those by the conventional image enhancement methods with respect to contrast improvement ratio (CIR) which was defined as an objective performance measure in this paper. The performance of the proposed method was also evaluated by means of the receiver operating-characteristics (ROC) analysis. The ROC analysis is based on statistical decision theory and has been applied extensively to the evaluation of clinical diagnosis [13], [14]. The ROC curve represents the relationship between the true-positive fraction (TPF) and the false-positive fraction (FPF) as the decision threshold varies. The area under the ROC curve, A_z, is used as an index of detection accuracy.

In Section II of this paper, the proposed method for mammographic image enhancement is presented in detail. Section III describes the performance measure used for evaluating the objective performance of the image enhancement methods. The evaluation results by the CIR and the ROC analysis are presented and discussed in Section IV followed by the conclusions in Section V.

II. Adaptive Image Enhancement Method

Fig. 1 shows the block diagram of the proposed method for mammographic image enhancement. At first, a simple film-artifact removal filter is applied to the mammographic image in order to remove the film-artifacts. There are small emulsion continuity faults on the X-ray mammogram films, which look like microcalcifications [15]. These artifacts are usually sharply defined and brighter than the microcalcifications, and the size of the artifacts is within 3×3 pixels in our experiments.

Let us consider two windows centered on a current pixel (x, y) as shown in Fig. 2. In Fig. 2, R_1 is the inner region and R_2 is the surrounding region. If the difference between the pixel value at the current position (x, y) and the mean value of the surrounding region is larger than a threshold value, T, the

Manuscript received May 21, 1996; revised March 7, 1997. The Associate Editor responsible for coordinating the review of this paper and recommending its publication was L. P. Clarke. *Asterisk indicates corresponding author*.

J. K. Kim is with the Department of Information and Communication Engineering, Korea Advanced Institute of Science and Technology, Dongdaemungu, Seoul 130-012, Korea.

J. M. Park and K. S. Song are with the Department of Diagnostic Radiology, Asan Medical Center, University of Ulsan College of Medicine, Songpagu, Seoul 138-040 Korea.

*H. W. Park is with the Department of Information and Communication Engineering, Korea Advanced Institute of Science and Technology, 207-43 Cheongryangri, Dongdaemungu, Seoul 130-012, Korea (e-mail: hwpark@athena.kaist.ac.kr).

Publisher Item Identifier S 0278-0062(97)07582-4.

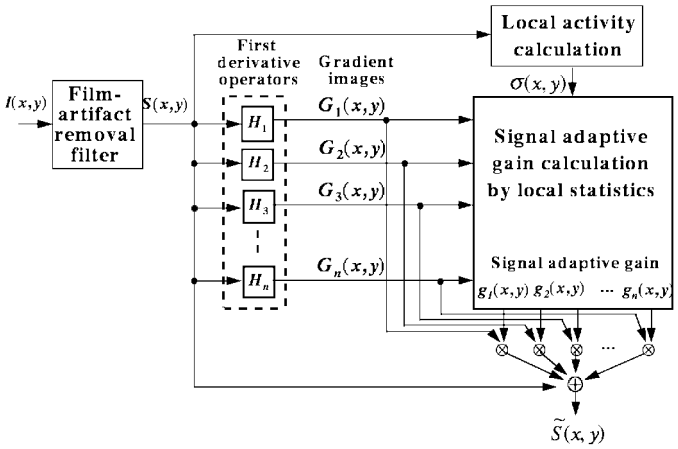

Fig. 1. Block diagram of the proposed adaptive enhancement method. $G_k(x, y)$ and H_k are the kth gradient images and the corresponding first derivative kernels, respectively, and $g_k(x, y)$ is the signal-adaptive gain for kth gradient image and $\sigma(x, y)$ is the local standard deviation of the filtered image $S(x, y)$. n is the number of kernels for the first derivative operations. For example, 3×3 Sobel operators have two kernels, whereas 3×3 compass operators have four kernels.

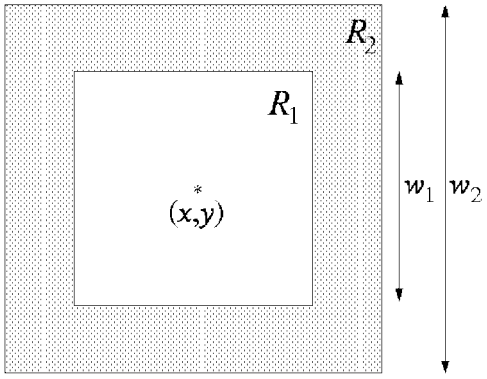

Fig. 2. Configuration of film-artifact removal filter. R_1 and R_2 are the inner region and the surrounding region, respectively. w_1 and w_2 denote the size of each square window. In this study, w_1 and w_2 are three and five, respectively.

pixel value of current position is substituted by the mean value of the surrounding region R_2. The output of the film-artifact removal filtering, $S(x, y)$, is defined as

$$S(x, y) = \begin{cases} A(x, y), & \text{if } [I(x, y) - A(x, y)] > T \\ I(x, y), & \text{otherwise} \end{cases} \quad (1)$$

where $I(x, y)$ is the digitized original image and $A(x, y)$ is the mean value of the surrounding region R_2 centered at (x, y). In (1), the threshold value, T, is empirically selected from many digitized mammograms so that the film-artifacts can be removed and the microcalcifications can be preserved.

After removal of the film-artifacts, the image $S(x, y)$ is enhanced by adding the adaptively weighted gradient images as follows:

$$\tilde{S}(x, y) = S(x, y) + \sum_{k=1}^{n} g_k(x, y) G_k(x, y) \quad (2)$$

where $\tilde{S}(x, y)$ is the enhanced image, n is the number of kernels for the first derivative operations, and $g_k(x, y)$ is the signal-adaptive gain for kth gradient image. In (2), $G_k(x, y)$ is the gradient image obtained by convolving the image $S(x, y)$ with kth kernel of the first derivative operators such as the Sobel operators or the compass operators. Fig. 3 describes two kernels of the Sobel operators and four kernels of the compass operators. The enhanced image, $\tilde{S}(x, y)$ may have large value than the maximum gray level or negative value in (2). Therefore, rescaling process should be performed so that the enhanced image has positive values which are less than or equal to the maximum gray level.

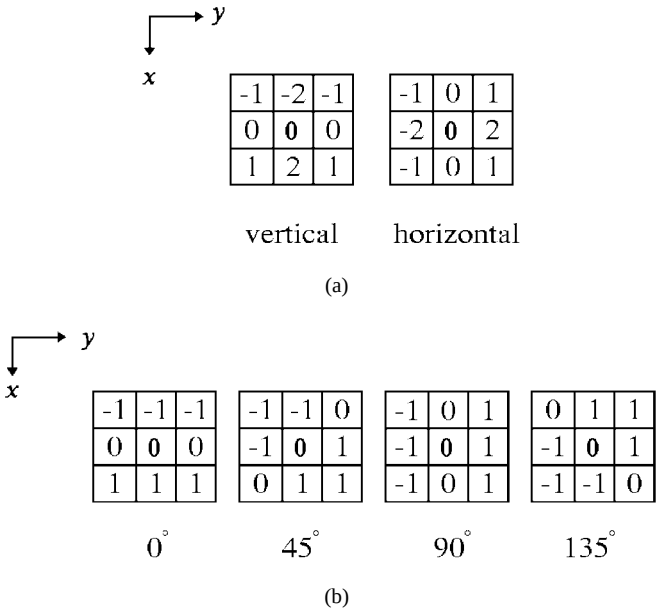

Fig. 3. Descriptions of the kernels for the first derivative operators: (a) the Sobel operators and (b) the compass operators. Bolded element indicates the location of the origin.

The signal-adaptive gain, $g_k(x, y)$, which adaptively weights the gradient images at the current pixel (x, y), is given as

$$g_k(x, y) = \begin{cases} -\dfrac{g_k^{\max}(x, y) - 1}{\sigma_0^{\max}} \sigma(x, y) + g_k^{\max}(x, y), & \text{if } e(x, y) = 1 \\ 1, & \text{if } e(x, y) = 0 \end{cases}$$
$$\text{for } k = 1, 2, \cdots, n \quad (3)$$

where $\sigma(x, y)$ is the local standard deviation of the filtered image $S(x, y)$ with a proper window size centered on the current pixel (x, y), $\sigma_0^{\max}$ is the maximum value of the local standard deviation in an image, and $g_k^{\max}(x, y)$ is the maximum gain corresponding to the pixel location (x, y) of kth gradient image. In (3), $e(x, y)$ is the binary edge value defined by the nonmaximum deletion algorithm [16], which is described in the end of this section. To improve the visibility of mammographic lesions of low contrast, the signal-adaptive gain is large for edges in the nonbusy regions where the local standard deviation is small, whereas the gain is small for the busy region.

The maximum gain, $g_k^{\max}(x, y)$, at the pixel location (x, y) of kth gradient image is computed as (4) (shown at the

bottom of the page) where σ_{G_k} and m_{G_k} are the global standard deviation and the global mean of kth gradient image, respectively, and $\sigma_G^{\max} = \max_k \{\sigma_{G_k},\ 1 \le k \le n\}$. If the pixel value of gradient image is within one-sigma region, it can be regarded as the uniform region in (4).

In order to apply the nonmaximum deletion algorithm for the binary edge value $e(x, y)$, the gradient magnitude and direction should be defined at each point (x, y). For the 3 $\times$ 3 Sobel operators, the magnitude and the direction of the gradient vector at a pixel (x, y) are measured as follows:

$$M(x, y) = \sqrt{G_1(x, y)^2 + G_2(x, y)^2} \tag{5}$$

$$\theta(x, y) = \tan^{-1} \frac{G_2(x, y)}{G_1(x, y)} \tag{6}$$

where $G_1(x, y)$ and $G_2(x, y)$ are the gradient images obtained by the vertical and the horizontal directional kernels as shown in Fig. 3(a), respectively. The direction of (6) should be quantized to eight typical directions such as 0°, ±45°, ±90°, ±135°, and 180° in order to apply the nonmaximum deletion algorithm. For the 3 × 3 compass operators, the magnitude and the direction of gradient vector at a pixel (x, y) are measured as follows:

$$M(x, y) = \max_k \{|G_k(x, y)|\}, \qquad \text{for } k = 1, 2, 3, \text{ and } 4 \tag{7}$$

$$\theta(x, y) = \text{the direction of kernel with maximum magnitude} \tag{8}$$

where $G_1(x, y)$, $G_2(x, y)$, $G_3(x, y)$, and $G_4(x, y)$ are the gradient images obtained by 0°, 45°, 90°, and 135° directional kernels of compass operators, respectively, as shown in Fig. 3(b). In (6) and (8), the angles are defined with respect to the x axis in Fig. 3.

A 3 × 1 window is placed along the gradient direction centered on the current pixel (x, y). The binary edge value, $e(x, y)$, is defined as follows:

$$e(x, y) = \begin{cases} 1, & \text{if } M(x, y) \text{ is maximum in the } 3 \times 1 \text{ window along } \theta(x, y) \\ 0, & \text{otherwise.} \end{cases} \tag{9}$$

As shown in (2), (3), and (9), the pixel points corresponding to the local maxima are more enhanced than the other points to improve the visual quality.

III. Performance Measure of Enhancement

The quantitative measurement of the contrast improvement is often very difficult. Moreover, there is no universal measure specifying both the objective and the subjective validity of an enhancement method. The contrast is usually defined as the difference in mean luminances between an object and its surroundings. In practice, there are many definitions of the contrast measure [7], [17]. When an image is composed of textured regions such as mammographic images, it seems more desirable to define the local contrast. The local contrast proposed by Gordon and Rangayyan [5] was defined by the mean gray values in two rectangular windows centered on a current pixel (x, y). Beghdadi and Negrate [17] proposed another definition of the local contrast based on local edge information of the image in order to improve the definition of Gordon and Rangayyan.

This paper adopts the local contrast proposed by Beghdadi and Negrate in order to define a performance measure of enhancement. The local contrast, $c(x, y)$, is defined as follows:

$$c(x, y) = \frac{|S(x, y) - \overline{E}(x, y)|}{S(x, y) + \overline{E}(x, y)} \tag{10}$$

where the mean edge gray level $\overline{E}(x, y)$ is measured by

$$\overline{E}(x, y) = \frac{\sum_{(x', y') \in W} \Delta(x', y') S(x', y')}{\sum_{(x', y') \in W} \Delta(x', y')} \tag{11}$$

where W is the window, whose size is an odd number in order to be centered on the current pixel (x, y) and is sufficiently large to filter out the noise and to preserve small details. In this paper, W was set to 7 × 7. In (11), the edge value $\Delta(x', y')$ is computed at each pixel (x', y') belonging to W. $\Delta(x', y')$ is the absolute difference between the gray level of pixel (x', y') and the mean gray level of the eight nearest neighbor pixels of (x', y'). The mean edge gray level $\overline{E}(x, y)$ is the average value of the gray levels at every edge points within the window W centered on the location (x, y). According to the definition in (10), when the considered pixel point lies on the object boundaries or on the uniform regions, the local contrast is small, whereas the vicinity of object boundaries has large local contrasts [17].

This paper proposes a performance measure of contrast improvement, namely the CIR, which is the ratio of the SSDC and the SSC within a region of interest (ROI) as follows:

$$\text{CIR} = \frac{\text{SSDC}}{\text{SSC}} = \frac{\sum_{(x, y) \in R} [c(x, y) - \tilde{c}(x, y)]^2}{\sum_{(x, y) \in R} c(x, y)^2} \tag{12}$$

$$g_k^{\max}(x, y) = \begin{cases} \dfrac{\sigma_G^{\max}}{\sigma_{G_k}} + \dfrac{\sigma_{G_k}}{\sigma_{G_1} + \sigma_{G_2} + \cdots + \sigma_{G_n}}, & \text{if } m_{G_k} - \sigma_{G_k} \le G_k(x, y) \le m_{G_k} + \sigma_{G_k} \\ \dfrac{\sigma_G^{\max}}{\sigma_{G_k}}, & \text{otherwise} \end{cases}$$
$$\text{for } k = 1, 2, \cdots, n \tag{4}$$

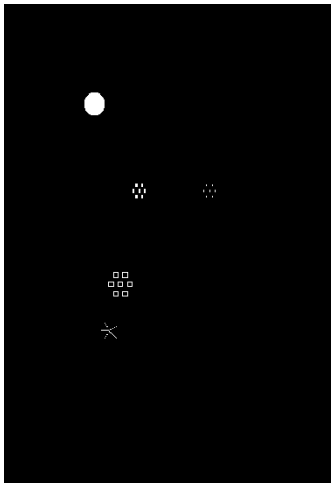

Fig. 4. Phantom features of similar shapes and sizes to real mammographic lesions. From top to bottom; well-circumscribed mass, clustered microcalcifications, minute clustered microcalcifications, circular calcifications, and stellate lesion.

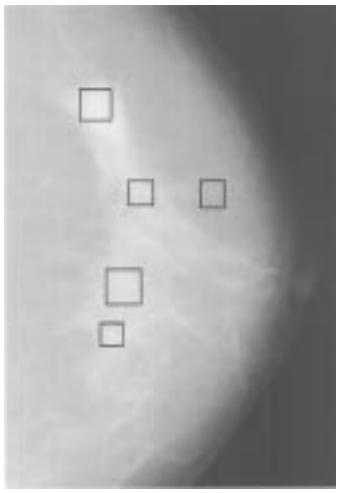

Fig. 5. Simulated image which was constructed by blending lowpass-filtered phantom features to a cancer-free mammogram.

where $c(x, y)$ and $\tilde{c}(x, y)$ are the local contrast values at (x, y) of the original image and the enhanced image, respectively. In (12), R is an ROI including each lesion.

IV. Evaluations of the Image Enhancement

A. Contrast Improvement Ratio

For the objective evaluation of the contrast improvement, the proposed method was compared with the three conventional enhancement methods such as the direct contrast enhancement, the adaptive histogram equalization, and the unsharp masking. The direct contrast enhancement [4], [5], [17] is based on the local contrast measure associated to each pixel and its contrast enhancement function. The method of Beghdadi and Negrate [17] is used in the experiment, which is based on local edge information of the image as shown in (10). The window size is 7×7 in order to compute the local contrast at the current pixel (x, y) and the exponential function is used for a contrast enhancement function. The adaptive histogram equalization [11], [18] enhances each pixel based on the histogram equalization of pixels within a region (i.e., a moving window) surrounding the pixel. In this experiment, the size of the moving window is 64×64 pixels. The unsharp masking [10] adds the gradient value weighted by the contrast gain to the original image. A commonly used gradient function is the Laplacian operator. In this experiment, the contrast gain has a value of five.

TABLE I
Comparisons of the SSC and the CIR for ROI's Including Phantom Features: (a) Direct Contrast Enhancement, (b) Adaptive Histogram Equalization, (c) Unsharp Masking, (d) Proposed Method with Sobel Operators, and (e) Proposed Method with Compass Operators

Phantom Features	SSC	CIR				
		a	b	c	d	e
Minute clustered micro-calcifications	0.0273	21.9510	47.4751	27.0098	54.1201	75.9967
Clustered microcalcifications	0.0202	14.6057	11.2552	12.0864	42.5563	69.1034
Stellate lesion	0.0320	13.8417	10.1532	23.6666	31.0721	36.3855
Circular calcifications	0.0216	14.2217	30.3762	19.1547	54.5319	67.9542
Well-circumscribed mass	0.0089	11.0017	2.0661	14.7933	33.2450	55.5978

A simulated image was constructed, which consisted of a mammographic image superimposed with phantom features of similar shapes and sizes to real lesions such as microcalcifications, stellate object, and well-circumscribed mass. The phantom features are shown in Fig. 4. These phantom features of the small amplitudes were smoothed by lowpass filtering and then blended into a clinically proven cancer-free mammographic image as shown in Fig. 5. A cancer-free X-ray mammogram was digitized with a pixel size of 180×180 μm^2 and 12b/pixel using a LUMISYS laser film digitizer. This image was cropped to a matrix size of 512×512 and then quantized to 8b per pixel for this experiment.

Fig. 6(a) shows the image enhanced by the direct contrast enhancement. The enhanced images from the adaptive histogram equalization and the unsharp masking are shown in Fig. 6(b) and (c), respectively. Fig. 6(d) and (e) shows the images enhanced by the proposed method with the Sobel operators and the compass operators, respectively. In Figs. 5 and 6, the rectangular marks are to denote the ROI for computing the CIR. Table I shows the comparison results of SSC and CIR for ROI's including phantom features as shown in Figs. 5 and 6. In all phantom features, the proposed method shows the best performance among the other methods with respect to the CIR. Fig. 7 shows the magnified areas containing each phantom feature in the enhanced images of Fig. 6. The images in Fig. 7 were magnified by the two-dimensional (2-D) bilinear interpolation method. Because the proposed method makes the visual observation easier than the other methods by the shadowing effects as shown in Figs. 6 and 7, it helps radiologists identify the real lesions.

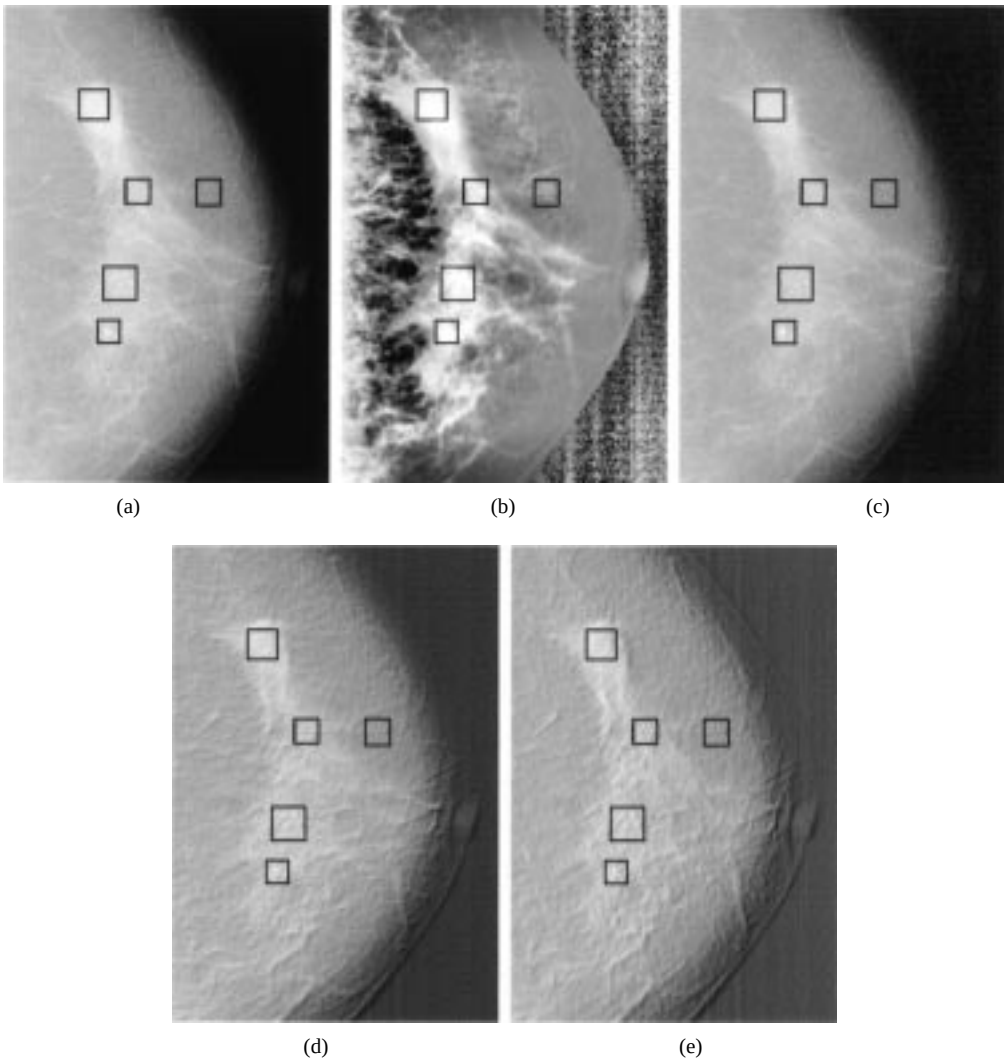

Fig. 6. The simulated images enhanced by several enhancement methods: (a) direct contrast enhancement, (b) adaptive histogram equalization, (c) unsharp masking, (d) proposed method with Sobel operators, and (e) proposed method with compass operators.

TABLE II
COMPARISONS OF THE SSC AND THE CIR FOR ROI'S INCLUDING REAL CLUSTERED MICROCALCIFICATIONS: (a) DIRECT CONTRAST ENHANCEMENT, (b) ADAPTIVE HISTOGRAM EQUALIZATION, (c) UNSHARP MASKING, (d) PROPOSED METHOD WITH SOBEL OPERATORS, AND (e) PROPOSED METHOD WITH COMPASS OPERATORS. CASES 1–7 ARE THE ROI'S INCLUDING CLUSTERED MICROCALCIFICATIONS WHICH ARE SHOWN IN FIG. 8 FROM TOP TO BOTTOM, RESPECTIVELY

Real Lesions	SSC	CIR				
		a	b	c	d	e
Case 1	0.1482	6.1266	1.9398	15.0368	24.6465	29.9928
Case 2	1.0471	3.5203	5.9333	3.0178	15.6529	16.7715
Case 3	0.1554	5.1730	22.0628	3.7983	14.4424	24.7296
Case 4	0.1777	4.9308	8.6064	3.4642	13.4992	24.1418
Case 5	0.0690	6.2780	5.8597	3.5038	12.4351	29.1651
Case 6	0.2981	5.1558	4.6636	4.6267	6.0454	7.5288
Case 7	0.0875	4.9585	7.5437	3.8506	13.9318	15.1622

As shown in Figs. 6 and 7, the proposed method using Sobel operators or compass operators cannot enhance the edge of some directions. The reason of this phenomenon is as follows: The gradient value of the edge where the pixel values vary from black to white is positive, whereas it is negative where the pixel values vary from white to black. Therefore, these positive and negative values of a gradient image describe the enhanced image as object shadow illustrated by unidirectional parallel light source which is located at $-135°$ with respect to the x axis for the Sobel operators and $-112.5°$ with respect to the x axis for the compass operators. This phenomenon makes a specific directional edge nonvisible; the enhanced image from the Sobel operators cannot enhance the edge whose gradient direction is $45°$ or $-135°$, whereas the enhanced image from the compass operators cannot enhance the edge whose gradient direction is $67.5°$ or $-112.5°$.

The comparative studies of CIR were also performed for the selected seven mammographic images containing real clustered microcalcifications, which were digitized with a pixel size of 180×180 μm^2 and 12b/pixel. Fig. 8 shows the magnified areas containing clustered microcalcifications in the enhanced images. The enhancement process was performed on 12-b gray levels. The images in Fig. 8 were also magnified by the 2-D bilinear interpolation method. Table II shows the comparison results of SSC and CIR for ROI's including clustered microcalcifications. In real clustered microcalcifications,

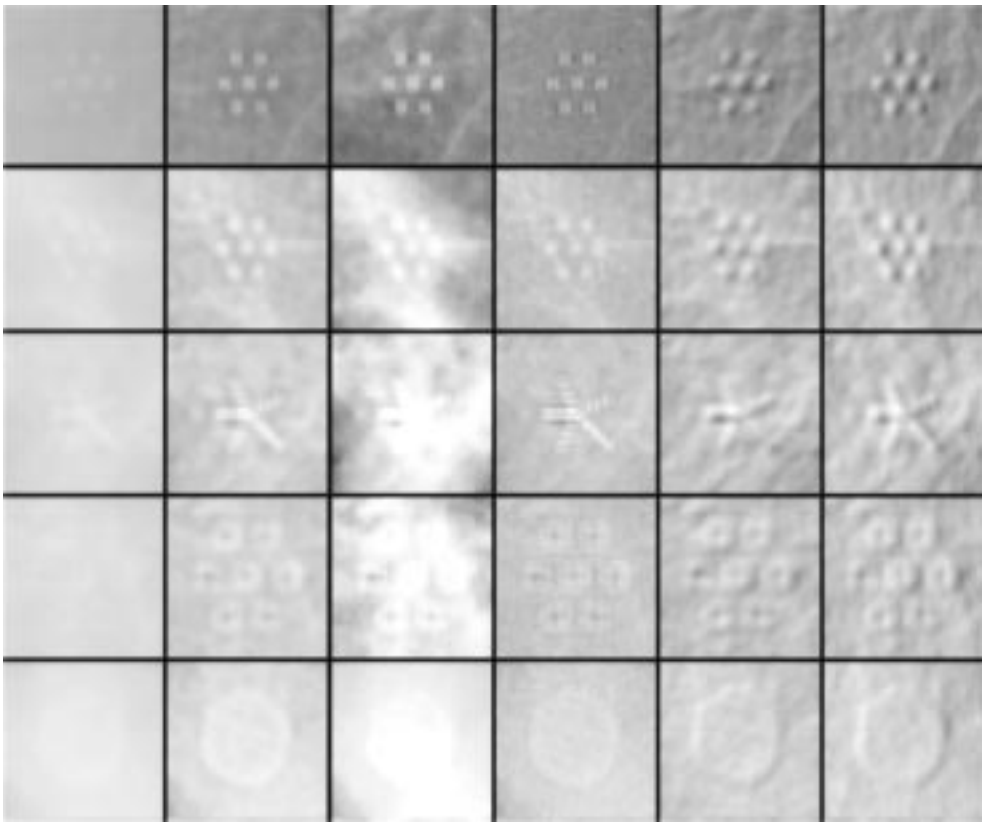

(a) (b) (c) (d) (e) (f)

Fig. 7. Contrast enhancement for each phantom feature magnified by the 2-D bilinear interpolation method. From top to bottom; minute clustered microcalcification, clustered microcalcification, stellate lesion, circular calcification, and well-circumscribed mass: (a) original image, (b) direct contrast enhancement, (c) adaptive histogram equalization, (d) unsharp masking, (e) proposed method with Sobel operators, and (f) proposed method with compass operators.

the proposed method also shows the best performance among the other methods with respect to CIR.

B. ROC Analysis

For the real clinical application, the performance of the proposed method was evaluated by means of the ROC analysis. Seventy-eight X-ray mammograms were selected for this study by an expert mammographer, who did not perform this evaluation study. Fifty cases among 78 mammograms contain the subtle or obvious clustered microcalcifications which were detected by the expert mammographer. The mammograms were digitized with a laser film digitizer (LUMISCAN 150) at a pixel resolution of 180 $\times$ 180 μm^2 and 12-b gray levels. Because of the large memory space and the long processing time for the entire mammogram, a region with 580 $\times$ 900 pixels which contained the breast region was selected for this study. The enhancement process was performed on 12b/pixel. The digitized mammograms were displayed on a 21-in high-contrast monochrome monitor which had the spatial resolution of 1760 $\times$ 2180.

To evaluate the detectability of the microcalcifications, three experienced radiologists read three different image sets, such as the digitized original images (image set 1, I_1), the enhanced images without film-artifact removal (image set 2, I_2), and the enhanced images with film-artifact removal (image set 3, I_3). To reduce reading-order effects [14], the ROC study was performed in two reading sessions on separate days for each radiologist. Seventy-eight mammograms were partitioned into two parts (part 1 and part 2) for two reading sessions. Each part consisted of 39 images containing 14 normal images and 25 abnormal images. Each reading session had three image sets of part 1 or part 2. For example, first session has I_1 of part 1, I_2 of part 2, and I_3 of part 1, and second session has I_1 of part 2, I_2 of part 1, and I_3 of part 2. During each session, the reading order of the images within each image set was varied randomly. Three experienced radiologists reported their confidence regarding the presence of clustered microcalcifications on five-category rating scale [13] such as: 1) definitely absent, 2) probably absent, 3) possibly present, 4) probably present, and 5) definitely present. Reading time was confined to 5s/image.

The pooled ROC curves for three different image sets are shown in Fig. 9, which were fitted by the ROCFIT developed by Metz *et al.* [14]. The pooled ROC curve was measured to average the results of three radiologists who have similar clinical experiences [19]. According to the area, A_z, under the ROC curve of Fig. 9, the enhanced images have improvements of the diagnostic performance of mammogram.

The CORROC2 developed by Metz *et al.* [20] was employed to test the statistical significance of the difference between two ROC curves, where bivariate chi-square test was applied to the simultaneous difference between the "a"

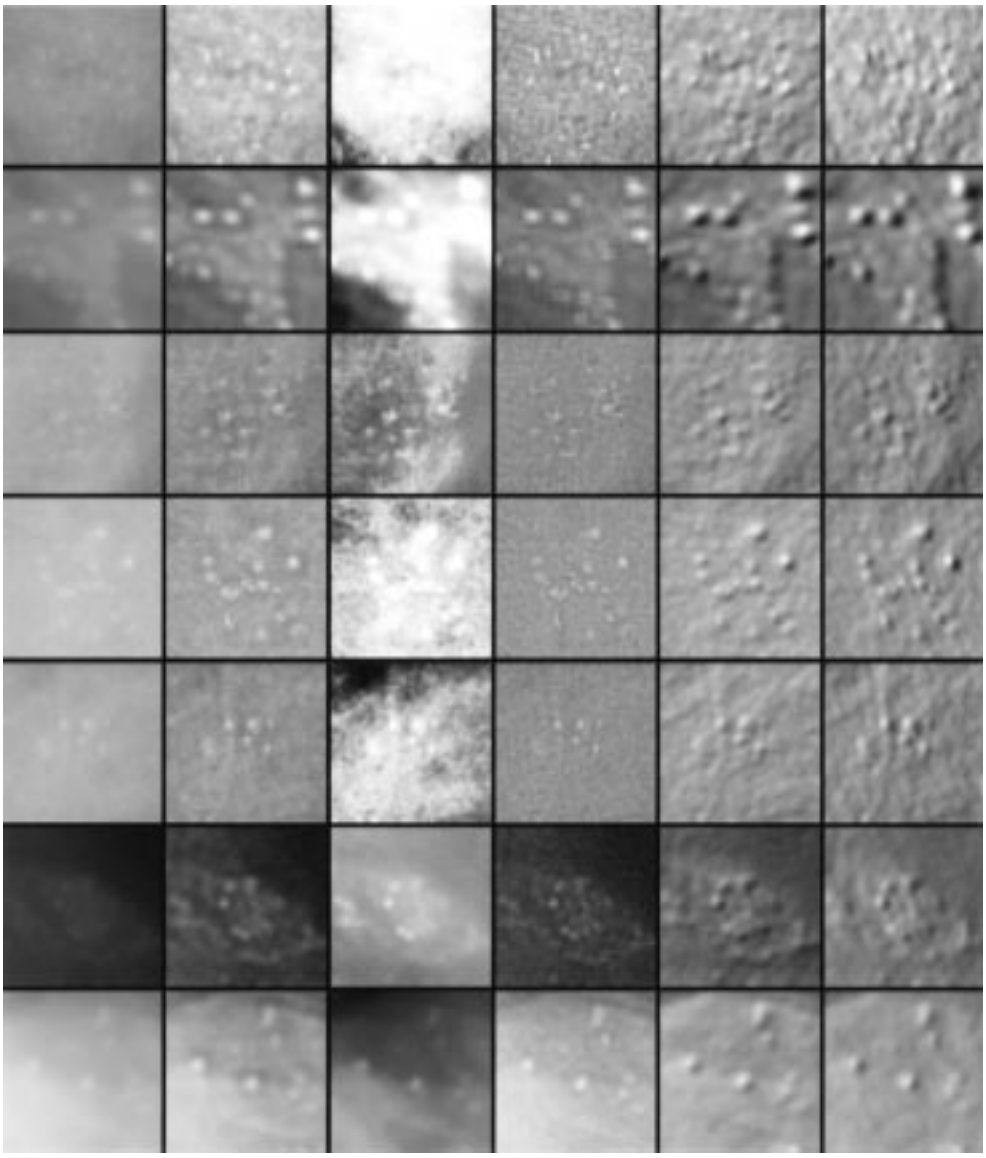

(a) (b) (c) (d) (e) (f)

Fig. 8. Contrast enhancement for seven real clustered microcalcifications magnified by the 2-D bilinear interpolation method: (a) original image, (b) direct contrast enhancement, (c) adaptive histogram equalization, (d) unsharp masking, (e) proposed method with Sobel operators, and (f) proposed method with compass operators.

parameters (y-intercept on normal-deviate axes) and between the "b" parameters (the slope of the straight line on normal-deviate axes) of the two ROC curves. Table III shows the areas, A_z, under the individual radiologist's ROC curves for each image set, which were fitted by the ROCFIT, and p-levels corresponding to the statistical significance of the difference for every pair of image sets. As shown in Table III, the improvement of A_z for the enhanced images with film-artifacts removal is statistically significant at the $p < 0.05$ level in comparison with the original images for the three radiologists. The difference between the enhanced images with film-artifact removal and the enhanced images without film-artifact removal is also statistically significant at the $p < 0.05$ level for the three radiologists. However, the difference between the enhanced images without film-artifact removal and the original images is not significant for the three radiologists. Because the film-artifacts adversely affect the performance by increasing the false-positive rate as shown in Fig. 9, the film-artifacts should be removed in the first stage of the image enhancement process.

V. Conclusions

This paper proposed an adaptive image enhancement method using first derivative and local statistics and showed the validity of detection of mammographic lesions. For the comparison study, a simulated image was designed, which consisted of a mammogram superimposed with similar features to real mammographic lesions. The performance of the proposed method was compared with those of the conventional enhancement methods with respect to the newly defined performance measure, CIR. The proposed method provided good results with respect to CIR for a simulated image and

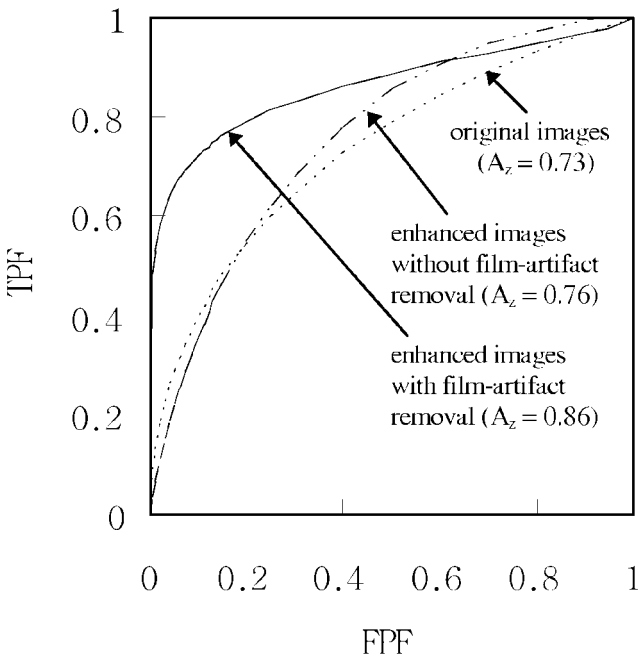

Fig. 9. Composite ROC curves for the three image sets obtained from the radiologist performance study. TPF and FPF denote the true-positive fraction and the false-positive fraction, respectively.

TABLE III
THE AREAS, A_z, UNDER THE INDIVIDUAL RADIOLOGIST'S ROC CURVES FOR EACH IMAGE SET AND p-LEVELS CORRESPONDING TO THE STATISTICAL SIGNIFICANCE OF THE DIFFERENCE FOR EVERY PAIR OF IMAGE SETS. THE IMAGE SET 1 (I_1) IS THE DIGITIZED ORIGINAL IMAGES, THE IMAGE SET 2 (I_2) IS THE ENHANCED IMAGES WITHOUT FILM-ARTIFACT REMOVAL, AND THE IMAGE SET 3 (I_3) IS THE ENHANCED IMAGES WITH FILM-ARTIFACT REMOVAL

	A_z			p-level		
Radiologist	I_1	I_2	I_3	I_3 vs. I_1	I_3 vs. I_2	I_2 vs. I_1
1	0.731	0.727	0.842	0.0384	0.0348	0.4711
2	0.724	0.764	0.858	0.0016	0.0432	0.3610
3	0.749	0.768	0.895	0.0178	0.0465	0.9382

the selected real mammograms with microcalcifications. The performance of the proposed method was also evaluated by means of the ROC analysis for the detection of real microcalcifications. The results of the ROC analysis has shown that the proposed method is effective in identifying the microcalcifications on digitized mammograms. With these promising results of the proposed method, it is necessary that further studies are performed to extend the proposed method into computer assisted diagnosis of mammograms.

REFERENCES

[1] R. G. Bird, R. G. Wallace, and B. C. Yankaskas, "Analysis of cancers missed at screening mammography," *Radiol.*, vol. 184, pp. 613–617, 1992.
[2] P. C. Johns and M. J. Yaffe, "X-ray characterization of normal and neoplastic breast tissues," *Phys. Med. and Biol.*, vol. 32, no. 6, pp. 675–695, 1987.
[3] D. B. Kopans, *Breast Imaging.* Philadelphia, PA: Lippincoff, 1989.
[4] A. P. Dhawan, G. Buelloni, and R. Gordon, "Enhancement of mammographic features by optimal adaptive neighborhood image processing," *IEEE Trans. Med. Imag.*, vol. MI-5, no. 1, pp. 8–15, 1986.
[5] R. Gordon and R. M. Rangayyan, "Feature enhancement of film mammograms using fixed and adaptive neighborhood," *Appl. Opt.*, vol. 23, no. 4, pp. 560–564, 1984.
[6] P. G. Tahoces, J. Correa, M. Souto, C. Gonzalez, L. Gomez, and J. J. Vidal, "Enhancement of chest and breast radiographs by automatic spatial filtering," *IEEE Trans. Med. Imag.*, vol. 10, no. 3, pp. 330–335, 1991.
[7] W. M. Morrow, R. B. Paranjape, R. M. Rangayyan, and J. E. L. Desautels, "Region-based contrast enhancement of mammograms," *IEEE Trans. Med. Imag.*, vol. 11, no. 3, pp. 392–406, 1992.
[8] W. Qian, L. P. Clarke, M. Kallergi, and R. A. Clark, "Tree-structured nonlinear filters in digital mammography," *IEEE Trans. Med. Imag.*, vol. 13, no. 1, pp. 25–36, 1994.
[9] A. F. Laine, S. Schuler, J. Fan, and W. Huda, "Mammographic feature enhancement by multiscale analysis," *IEEE Trans. Med. Imag.*, vol. 13, no. 4, pp. 725–740, 1994.
[10] A. K. Jain, *Fundamentals of Digital Image Processing.* Englewood Cliffs, NJ: Prentice-Hall, 1989.
[11] R. C. Gonzalez and R. E. Woods, *Digital Image Processing.* Reading, MA: Addison-Wesley, 1992.
[12] G. S. Robinson, "Edge detection by compass gradient masks," *Comput. Graphics, Image Processing*, vol. 6, pp. 492–501, 1977.
[13] C. E. Metz, "ROC methodology in radiologic imaging," *Investigative Radiol.*, vol. 21, no. 9, pp. 720–733, 1986.
[14] ———, "Some practical issues of experimental design and data analysis in radiological ROC studies," *Investigative Radiol.*, vol. 24, no. 3, pp. 234–245, 1989.
[15] G. Liszka, T. Roska, A. Zarandy, J. Hegyesi, L. Kek, and C. Rekeczky, "Mammogram analysis using CNN algorithms," in *Proc. SPIE*, 1995, vol. 2434, pp. 461–470.
[16] V. Lacroix, "A three-module strategy for edge detection," *IEEE Trans. Pattern Anal. Machine Intell.*, vol. 10, no. 6, pp. 803–810, 1988.
[17] A. Beghdadi and A. L. Negrate, "Contrast enhancement technique based on local detection of edges," *Comput. Vision, Graphics, Image Processing*, vol. 46, pp. 162–174, 1989.
[18] S. M. Pizer, E. P. Amburn, J. D. Austin, R. Cromartie, A. Geselowitz, T. Greer, B. H. Romeny, J. B. Zimmerman, *and K. Zuiderveld*, "Adaptive histogram equalization and its variations," *Comput. Vision, Graphics, Image Processing*, vol. 39, pp. 355–368, 1987.
[19] J. A. Swets and R. M. Pickett, *Evaluation of Diagnostic Systems: Methods from Signal Detection Theory.* New York: Academic, 1982.
[20] C. E. Metz, P. L. Wang, and H. B. Kronman, "A new approach for testing the significance of differences between ROC curves measured from correlated data," in *Information Processing in Medical Imaging: Proceedings of the 8th Conference.* Boston, MA: Martinus Nijhoff, 1984, pp. 432–445.